REPORT DOCUMENTATION PAGE

Form Approved
OMB No. 0704-0188

1. REPORT DATE *(DD-MM-YYYY)*	2. REPORT TYPE	3. DATES COVERED *(From - To)*
15-11-2011	Journal Article	

4. TITLE AND SUBTITLE

Reaction Cross Sections for Two DSMC Models: Accuracy and Sensitivity Analysis

5a. CONTRACT NUMBER

5b. GRANT NUMBER

5c. PROGRAM ELEMENT NUMBER

6. AUTHOR(S)
Ingrid Wysong, Sergey Gimelshein, Natalia Gimelshein, William McKeon, and Fabrizio Esposito

5d. PROJECT NUMBER

5f. WORK UNIT NUMBER
23080532

7. PERFORMING ORGANIZATION NAME(S) AND ADDRESS(ES)

Air Force Research Laboratory (AFMC)
AFRL/RZSA
10E. Saturn Blvd.
Edwards AFB CA 93524-7680

8. PERFORMING ORGANIZATION REPORT NUMBER

AFRL-RZ-ED-JA-2011-500

9. SPONSORING / MONITORING AGENCY NAME(S) AND ADDRESS(ES)

Air Force Research Laboratory (AFMC)
AFRL/RZS
5 Pollux Drive
Edwards AFB CA 93524-7048

10. SPONSOR/MONITOR'S ACRONYM(S)

11. SPONSOR/MONITOR'S NUMBER(S)
AFRL-RZ-ED-JA-2011-500

12. DISTRIBUTION / AVAILABILITY STATEMENT

Approved for public release; distribution unlimited (PA #11983).

13. SUPPLEMENTARY NOTES
For submission to the Journal: Physics of Fluids

14. ABSTRACT
The Quantum Kinetic chemical reaction model proposed by Bird for the direct simulation Monte Carlo method is based on collision kinetics with no assumed Arrhenius-related parameters. It demonstrates an excellent agreement with the best estimates for thermal reaction rates coefficients and with two-temperature nonequilibrium rate coefficients for high-temperature air reactions. This paper investigates this model further, concentrating on the non-thermal reaction cross sections as a function of collision energy, and compares its predictions with those of the earlier total collision energy model, also by Bird, as well as with available quasi-classical trajectory cross section predictions (this paper also publishes for the first time the complete sets of these computed reaction cross sections). A rarefied hypersonic flow over a cylinder is used to examine the sensitivity of the number of exchange reactions to the differences in the two models under a strongly nonequilibrium velocity distribution.

15. SUBJECT TERMS

16. SECURITY CLASSIFICATION OF:			17. LIMITATION OF ABSTRACT	18. NUMBER OF PAGES	19a. NAME OF RESPONSIBLE PERSON
					Andrew D. Ketsdever
a. REPORT	b. ABSTRACT	c. THIS PAGE	SAR	10	19b. TELEPHONE NUMBER *(include area code)*
Unclassified	**Unclassified**	**Unclassified**			N/A

Standard Form 298 (Rev. 8-98)
Prescribed by ANSI Std. 239.18

Reaction Cross Sections for Two DSMC Models: Accuracy and Sensitivity Analysis

Ingrid Wysong,[1] Sergey Gimelshein,[2] Natalia Gimelshein,[2] William McKeon,[2] and Fabrizio Esposito[3]
[1)] *AFRL/RZSA Edwards AFB, CA 93524*[a)]
[2)] *ERC Inc, Edwards AFB, CA 93524*
[3)] *IMIP of CNR, 70126 Bari, Italy*

(Dated:)

The Quantum Kinetic chemical reaction model proposed by Bird for the direct simulation Monte Carlo method is based on collision kinetics with no assumed Arrhenius-related parameters. It demonstrates an excellent agreement with the best estimates for thermal reaction rates coefficients and with two-temperature nonequilibrium rate coefficients for high-temperature air reactions. This paper investigates this model further, concentrating on the non-thermal reaction cross sections as a function of collision energy, and compares its predictions with those of the earlier total collision energy model, also by Bird, as well as with available quasi-classical trajectory cross section predictions (this paper also publishes for the first time the complete sets of these computed reaction cross sections). A rarefied hypersonic flow over a cylinder is used to examine the sensitivity of the number of exchange reactions to the differences in the two models under a strongly nonequilibrium velocity distribution.

PACS numbers: 02.70.Ns,47.70.Fw
Keywords: DSMC, reaction models, cross sections

I. INTRODUCTION

Modeling of chemical reactions in the direct simulation Monte Carlo (DSMC) method[1] has a 40-year long history. Starting from the simplest model with the probability described by a Heaviside step function and depending only on the line-of-centers collision energy, reaction models have grown over the years in their physical adequacy and sophistication. Many of them include such features as vibrational favoring and discrete internal energy modes. Nevertheless, the total collision energy (TCE) model[2] is still the most widely chemical reaction model in the DSMC community.

Generally, for a reaction model to be defined, it is necessary to identify the probability of chemical reaction as a function of the energy modes of the colliding pair and determine the after-reaction energy redistribution over energy modes of the reaction products. Of these two components, the more important is the probability of chemical reaction, usually defined as the ratio of the reaction cross section, that governs the rate of collisions leading to reaction, to the total collision cross section. The main difficulty in defining the reaction probability is related to the lack of experimental or theoretical estimates of energy-dependent reaction cross sections for almost all reactions of interest. Because of this, additional assumptions are used. In the TCE model mentioned above, the reaction cross section is assumed to be a function of the total collision energy (independent of the division of energy between translational and internal modes). The functional form is assumed to follow the reaction cross section obtained with the Laplace transform of the reaction rate equation for simple gases and the variable hard sphere (VHS) collision model for overall collision frequency.[3]

Although the TCE model has the advantage of matching a known equilibrium reaction rate in the extended Arrhenius form, it also has a number of disadvantages related to the above assumptions, such as the inability to include any type of internal mode favoring, reaction probability that may exceed unity for some reactions at high energies, and uncertainties related to the choice of model parameters. Therefore, a simple chemical reaction model with no adjustable parameters that produces reasonable thermal rate coefficients $k(T)$ for key rates look very appealing. Recent work[4–6] has presented the QK (Quantum Kinetic) approach to predicting rate coefficients, which has shown very promising results for temperature-dependent $k(T)$ for several reactions. It may be argued, however, that the energy-dependent reaction cross section $\sigma(E)$ may also be very important for highly nonequilibrium flows. In what follows, the behavior of the QK model is examined in terms of effective $\sigma(E)$ for two important air reactions. Existing quasi-classical trajectory (QCT) cross sections for N_2+N dissociation and for N_2+O endothermic exchange provide a good test case. A DSMC simulation of a simple axisymmetric hypersonic flow is also presented in order to examine the sensitivity of the number of reactions to variations in the model cross sections.

II. REACTION MODELS

The VHS collision model will be used in the flowfield simulations, but it is also needed to compute the reac-

[a)] Electronic mail: Ingrid.Wysong@edwards.af.mil

TABLE I. High temperature VHS parameters for air species collisions. Upper numbers, d_{ref} in Å, lower numbers, ω.

	N	O	N_2	O_2	NO
N	3.000	3.229	3.734	3.535	3.600
	0.75	0.75	0.75	0.76	0.77
O	3.229	3.458	3.360	3.764	3.829
	0.75	0.76	0.75	0.76	0.77
N_2	3.734	3.360	4.467	4.269	4.334
	0.75	0.75	0.75	0.76	0.765
O_2	3.535	3.764	4.120	4.070	4.135
	0.76	0.76	0.76	0.77	0.78
NO	3.600	3.829	4.334	4.135	4.200
	0.77	0.77	0.765	0.78	0.79

tion rate coefficient and cross section values. Since the focus here is high-temperature reacting flows, such as in a bowshock, VHS parameter values are selected that are reasonable for the high-temperature regime for the collision pairs (N_2-N and N_2-O) of interest. Literature predictions for the viscosity of air species-pairs by Capitelli[7] are used, and VHS parameters that match the defined viscosity in the 5,000 K to 15,000 K range are selected and shown in Table I. Note that though a reference temperature of $T_{ref} = 273$ K is used for convenience (since many DSMC codes use this T_{ref} value), the values of selected reference diameter d_{ref} and the exponent in the viscosity-temperature dependence ω produce the desired viscosity values at high temperatures and do not match known viscosities at lower temperatures.

The QK model described in Refs. 4–6 has the extremely attractive feature of having no adjustable parameters. The QK model first defines a collision energy E_c which is the sum of the translational energy of the collision and the vibrational energy of the molecular species. Rotational energy does not contribute to the reaction probability in this model. The QK model, like any other, will also need an input for the activation energy, E_a. For the two strongly endothermic reactions considered here, we have made the common simplifying assumption that E_a is equal to the heat of reaction. However, since some reactions (especially exothermic ones) have a non-negligible energy barrier, the QK model (like all others) in these cases would have to use an adjustable input value for the activation (barrier) energy derived from experiment. The rate coefficients resulting from this approach have been well documented, along with their favorable comparison with experimental values, in Refs. 4–6. The effective cross section from this approach depends on the inelastic collision model, and for the Larsen-Borgnakke[8] model with discrete vibrational energies and $E_c > E_a$ may be written as

$$\sigma(E_c) = \sigma_T(E_c) \cdot P = \sigma_T(E_c) \cdot \frac{\left(1 - \frac{i_a k \Theta_v}{E_c}\right)^{1.5-\omega}}{\sum_{i=0}^{i_a} \left(1 - \frac{ik\Theta_v}{E_c}\right)^{1.5-\omega}}, \quad (1)$$

TABLE II. TCE model parameters in SI units used for exchange and dissociation reactions.

Reaction	A	B	E_a	$\bar{\zeta}$
Dissociation	7.140×10^{-8}	-1.5	1.561×10^{-18}	2
Exchange (Bose)	5.690×10^{-12}	0.42	5.928×10^{-19}	2
Exchange (Bose refit)	7.680×10^{-22}	1.4	5.276×10^{-19}	2

where P is the reaction probability, $\sigma_T(E_c)$ is the total VHS/VSS collision cross section, Θ_v is the characteristic vibrational temperature, and $i_a = \left[\frac{E_a}{k\theta_v}\right]$. For the dissociation reactions, because the algorithm merely states that any collision that satisfies $E_c > E_a$ will dissociate (probability is equal to one), the resulting effective cross section takes a very simple form of 0 for $E_c < E_a$ and $\sigma_T(E_c)$ for $E_c > E_a$.

The TCE chemistry model is presented in Ref. 2 and matches given equilibrium Arrhenius rate coefficients in the limit of equilibrium conditions. In the limit of no internal energy, it is the exact Laplace transform cross section of the $k(T)$ rate written in the Arrhenius form $k(T) = AT^B \exp(-\frac{E_a}{kT})$. The values for the four adjustable parameters of the model used here are shown in Table II, where the Arrhenius parameters used are those given in Refs. 9 and 10 to match the QCT results for the thermal reaction rate coefficients. The fourth TCE parameter, $\bar{\zeta}$, defines the average number of internal energy degrees of freedom that are assumed to contribute to the reaction cross section; here, both internal energy modes of the N_2 reactant (rotation and vibration) are assumed to fully contribute. The E_c used for the TCE model is defined differently than that for the QK model above since it does include rotational energy. The TCE model used here differs slightly from that in Ref. 2 in that it uses quantized internal energy levels (Simple Harmonic Oscillator levels for vibration with zero-point energy) with the appropriate correction factor used in order to maintain the assumed $k(T)$.[11] Note that, since the TCE and QK models here use truncated-SHO energy levels while the QCT results of course use accurate anharmonic energy levels, we will be comparing cases where the TCE or QK vibrational energy is approximately equal to that for the QCT result, but the quantum number is different. Both DSMC models evaluate reaction probability on a per-collision-event basis and do not use macroscopic flow parameters.

III. DISSOCIATION CROSS SECTIONS

Consider first the N_2+N→N+N+N dissociation reaction. Reference 10,14 present the details of the QCT results by Esposito et al. using a semiempirical LEPS potential energy surface (PES). Although other recent PESs are more accurate for this reaction, published comparisons[15] with results obtained on these PESs in-

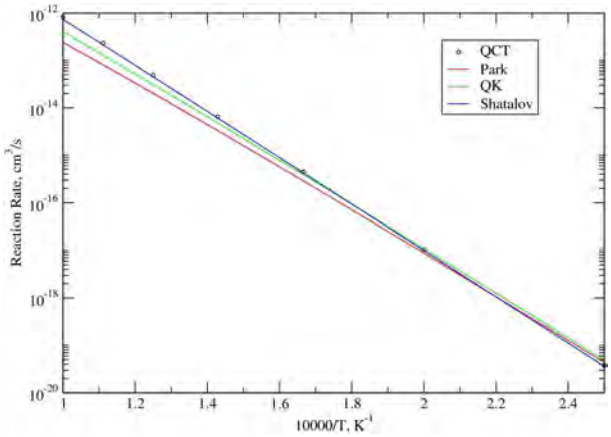

FIG. 1. Comparison of QK dissociation rates with QCT and experimental data of Ref.12 and Ref. 16.

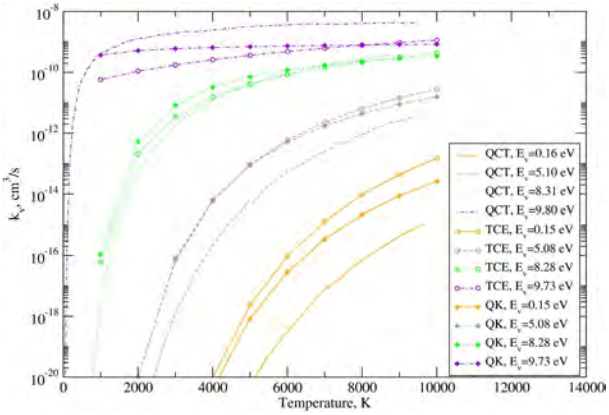

FIG. 2. Dissociation cross sections for different vibrational levels predicted by QK, TCE, and QCT models, as a function of translational-rotational temperature.

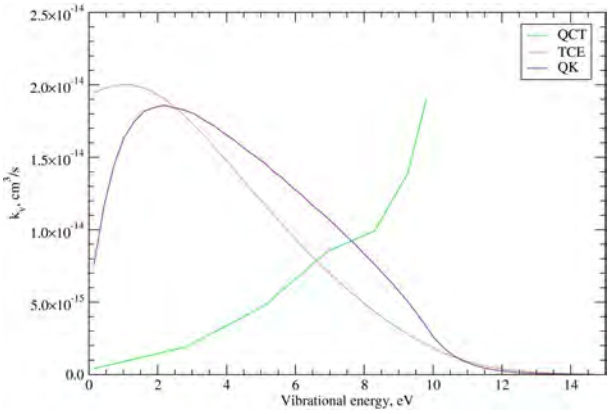

FIG. 3. Relative contributions of different vibrational levels to the reaction rate at 10,000 K as predicted by different models.

dicate that the reactive part of the vibration energy exchange processes is affected, and not the overall dissociation cross sections. For convenience and for archival purposes, the complete set of computed state-specific QCT dissociation cross sections are provided in a Supplementary Material Table III. Figure 1 shows the overall thermal rate coefficient for the two models and the QCT results. As already shown in Ref. 4, there is quite reasonable agreement between the QK model and the realistic QCT-obtained rate. Note that these theoretical rates are in good agreement with recommendations of Ref. 12 based on available experimental data, and the QCT is is excellent agreement with recent experimental data.[16] The TCE model agrees with the QCT rate by definition. Since many studies of dissociation models examine vibrational-state-specific rate coefficients $k_v(T)$, Fig. 2 shows some of these at a specific rotational-translational temperature varied between 300 K and 10,000 K. Both the QK and TCE models give good agreement with the QCT k_v at some intermediate values of vibrational energy ($E_v \approx 8$ eV), but are high for low v levels and low for high v levels. This qualitative difference is what is expected because the models makes the simplifying assumption that all forms of energy in the collision (translational, internal) contribute equally to the reaction, which is well known to be an invalid assumption for a diatomic dissociation reaction.

This point is made further in Fig. 3, which plots the relative contribution by each vibrational level to the overall reaction at a given equilibrium temperature (10,000 K); this contribution is given by the product of the k_v and the Boltzmann level population fraction. As expected, the QCT results show a strong vibrational favoring of the dissociation reaction[17], while the TCE and QK models display the "prior" unfavored distribution where the heavily-populated low-v levels dominate. Note that both DSMC models equally poorly compare to the QCT prediction; the presented temperature of 10,000 K is representative, and the results would qualitatively be similar for lower and higher temperatures. This result does not have direct implication for hypersonic rarefied flow where the degree of translational nonequilibrium is significant, and energy dependent cross sections need to be compared instead of temperature dependent rates. Such a comparison is presented in the end of this section.

The strong vibrational favoring of this dissociation reaction indicated by the QCT cross sections is illustrated in Fig. 4. For several example internal energy states, the computed cross section is plotted against the total collision energy (sum of vibrational, rotational and translational energy). At the same total energy, the cross section for a high vibrational level is orders of magnitude larger than that for a lower vibrational level; the difference increases for smaller collision energies. Because of the strong vibrational favoring, any simplified DSMC model that does not account for this effect (as is the case for both considered here) can at best only roughly simulate the reaction probabilities.

Finally, Fig. 5 shows sample QCT comparisons with DSMC cross sections. Figure 5 (left) shows a moderate vibrational level ($v = 9$ for the SHO models and $v = 10$

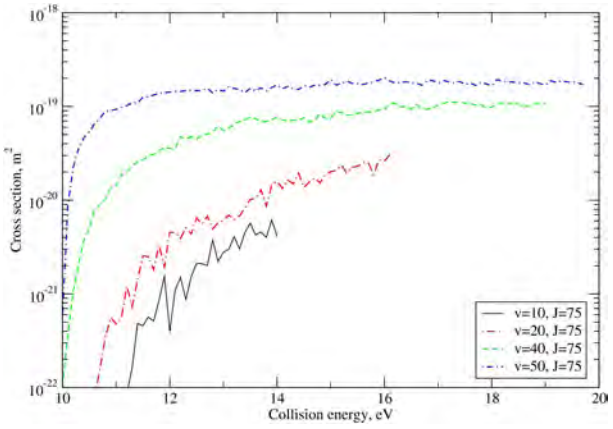

FIG. 4. Vibrational favoring in the dissociation reaction computed by QCT.

for the QCT result; both have about 2.8 eV of vibrational energy), and Fig. 5 (right) shows a very high vibrational level ($v = 33$ for the SHO models and $v = 60$ for the QCT result; both have about 9.8 eV of vibrational energy). The QK cross section is equal to the total collision (VHS) cross section for all translational energies sufficient to meet $E_c = E_t + E_v > E_a$; in other words, the reaction probability jumps from 0 to 1 for $E_c > E_a$. The difference between the QK cross section and the QCT for the high-v is due to the simplified VHS total collision model being somewhat lower than what is obtained by QCT with a realistic potential for the high-v levels. The TCE cross section shows a surprisingly close comparison to the QCT for the moderate-v and as expected is uniformly lower that the QCT for the high-v. For this moderate-v (lower-v cross sections are not available from the QCT results) the QK model is high by about two orders of magnitude and thus may be expected to significantly overestimate the dissociation probability in nonequilibrium flows with low vibrational excitation, such as high-altitude reentry type flows.

IV. EXCHANGE REACTION CROSS SECTIONS

Consider next the N_2+O→N+NO Zeldovich exchange reaction. It is critical in hypersonic air chemistry and thus has drawn significant attention in the literature, including a thorough set of QCT predictions.[9,20] For convenience and for archival purposes, the complete set of computed state-specific QCT exchange reaction cross sections are provided in a Supplementary Material Table IV. Table II shows the Arrhenius parameters recommended by Bose as providing the most accurate fit to his QCT thermal rates in the range 1,000–14,000 K. However, since the activation energy E_a is a critical parameter for any collision-energy-based model, we use here a slightly different set where we have fixed E_a/k at the commonly-used value of 38,218 K, the heat of reaction, instead of Bose's $E_a/k = 42,938$ K, to facilitate comparison with the other models. With the E_a value fixed, the parameters for A and B shown in Table II as the "Bose refit" values still produce a very good agreement for $k(T)$ with the Bose values in the temperature range of interest. These "Bose refit" Arrhenius values are used as the adjustable parameters for the TCE model and, again by definition, produce the specified $k(T)$ under equilibrium. In Fig. 6, the "Bose refit" and the QK results for $k(T)$ are plotted along with 2 data-based $k(T)$ values.[12,18] The QK k(T) results, as previously shown in Ref. 4, agree with data quite reasonably without an adjustable parameter.

Figure 7 shows some of the QCT state-specific cross sections. The cross sections are plotted versus the total collision energy (the sum of translational, rotational, and vibrational modes), so that a higher vibrational level at any fixed collision energy implies lower translational-rotational energy. For this reaction, vibrational favoring is a relatively small effect; a given E_c with varied fractions of the energy in vibration only changes the σ by two to three times (for the dissociation reaction, a change of over three orders of magnitude can be seen). Therefore, one can hope that a simplified DSMC model can reasonably capture the reaction probability behavior.

Let us now compare the DSMC and QCT reaction cross sections. TCE and QCT cross sections depend on translational, rotational, and vibrational energies of the colliding molecules, while QK does not include the rotational energy of colliders. To simplify the comparison, it is reasonable to analyze the cross sections varying energy in one of the three modes, while keeping the other two fixed. The cross sections for the three chemical reaction models under consideration are presented in Fig. 8 for a fixed relative translational energy of 4.5 eV and 0-th vibrational level, with the rotational level J of N_2 allowed to vary. The QK cross section, which does not depend on J, is fairly close to QCT values only at intermediate J's. The TCE model provides a closer match to the QCT σ. Even though it noticeably underpredicts QCT for very small rotational levels, it captures the shape of the cross section fairly well.

The exchange reaction cross sections for varying v and fixed E_t=3.5 eV and $J = 0$ are given in Fig. 9. Here again, the TCE model provides a noticeably better agreement with the QCT results than QK model. It captures the QCT slope well, but underpredicts it by about 0.1Å^2 for most of vibrational levels. The QK model is characterized by a much weaker dependence on vibrational level than the other two models; it agrees with the QCT model for $v \approx 7$.

The last set of cross sections compares the three models for two sets of internal states with varying translational energies. Similar to the previous cases, the TCE model reasonably represents the QCT results for most translational energies. while the shape of the QK model σ is notably unphysical, high by a factor of five near threshold.

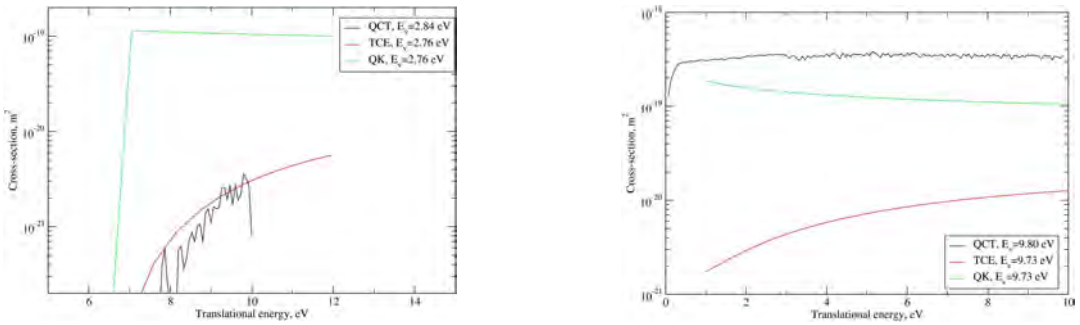

FIG. 5. Dissociation cross section as a function of translational energy E_t for low (left) and high (right) vibrational quantum states.

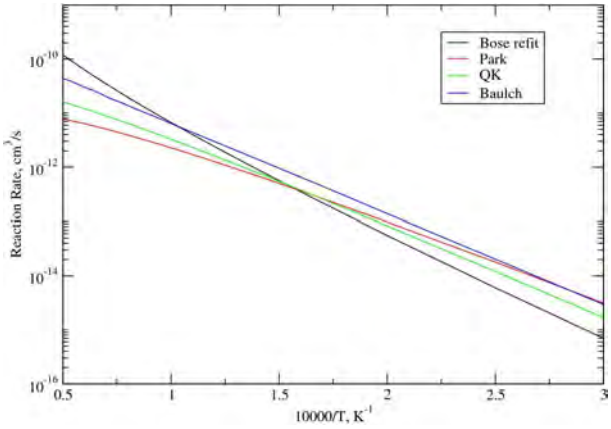

FIG. 6. Comparison of QK dissociation rates with QCT and experimental data of Ref. 12 and Ref. 18.

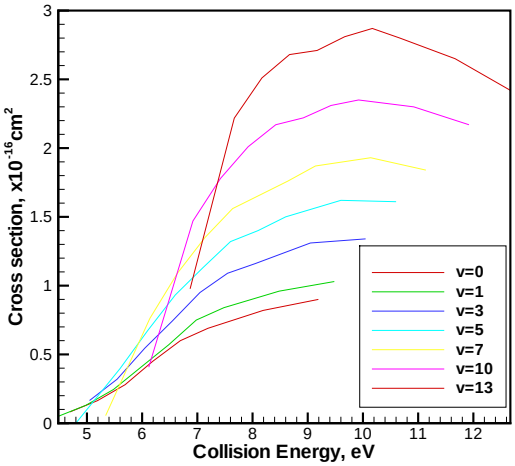

FIG. 7. QCT exchange reaction cross sections comparing various vibrational levels at given total collision energies, demonstrating weak vibrational favoring.

In order to make an initial assessment of the sensitivity of a highly nonequilibrium flowfield to the difference in these DSMC reaction models, we simulate a simple axisymmetric hypersonic flow over a cylinder using the SMILE code.[19] Since here we do not examine internal energy relaxation models or possible secondary reactions, an altitude of 120 km (freestream mole fractions: O, 17%, N_2, 74%, O_2, 8%) is selected so that the flow is in a nearly single-collision condition, and only the N_2+O exchange reaction will be detectable. Speeds of 8 km/s and 6 km/s were simulated and the QK and TCE models for the reaction were implemented with parameters as described above. For meaningful comparison, the QCT cross sections for the reaction were also used as an interpolated look-up table. The three models give nearly identical flow temperature results. For the 8 km/s case, 18,000 K peak translational temperature was observed in the shock and very low, about 1,100 K, N_2 rotational temperature; for the 6km/s case, these numbers are 11,000 K and 500 K, respectively. Figure 11 shows the difference in the NO reaction product mole fraction. While the TCE model closely agrees with the benchmark QCT case (6×10^{-6} and 6×10^{-4} for the 6 km/s and 8 km/s case, respectively), the QK model predicts an NO fraction too high by a factor of 3 to 5. Note that the thermal $k(T)$ for an

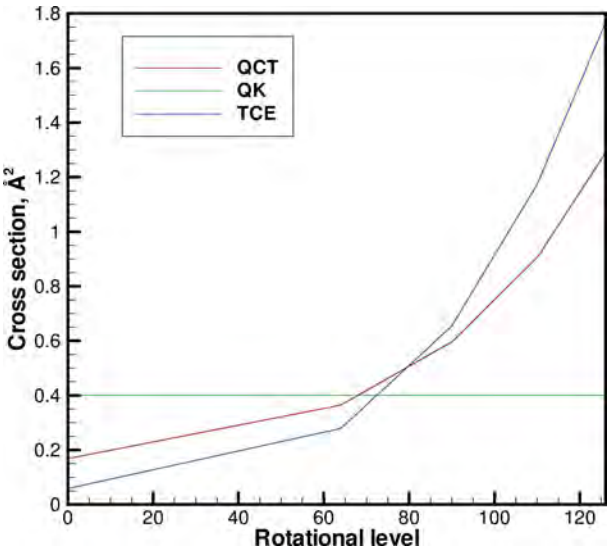

FIG. 8. Exchange reaction cross sections at fixed $E_t = 4.5$ eV and $v = 0$.

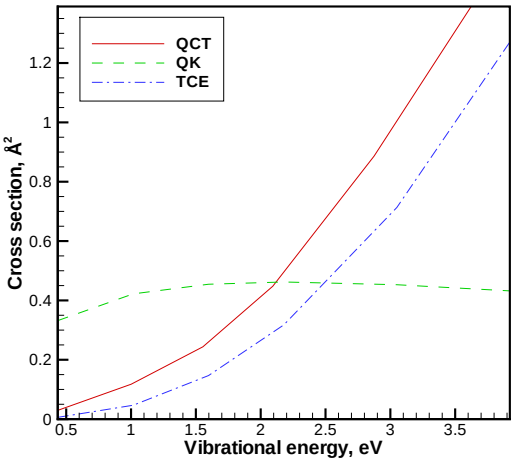

FIG. 9. Exchange reaction cross sections at fixed $E_t = 3.5$ eV and $J = 0$.

equilibrium temperature of 18,000K (see Fig. 6) of the QK is somewhat lower than the TCE and QCT (Bose) rate, but the number of reactions predicted by QK is actually higher in this flow due to the strong nonequilibrium and the unphysical shape of the QK cross section near threshold.

V. DISCUSSION AND CONCLUSIONS

It may be noted that, for reverse reactions, the QK model in its present form does not reproduce correct reaction equilibrium constants. However, recent work proposes modifications that can utilize adjustable parameters in the reverse reaction probabilities to produce correct equilibrium constants.[21] In summary, results that compare the proposed QK chemistry model with the earlier TCE model and with QCT results are presented for two important air reactions. This study is complementary to the previous studies[4,6] since the present focus is on the nonequilibrium aspects rather than on the equilibrium rate coefficients. As shown by the previous studies, the QK model, with no adjustable parameters, seems to produce impressively realistic $k(T)$ predictions for the reactions so far examined and thus should work well for near-equilibrium reacting flows. As shown here, for strongly nonequilibrium flows, the probability of reaction is sensitive to the shape of the energy-dependent cross section and the present results indicate that the QK model may not be well suited in this respect to simulate some reactions, such as a strongly endothermic reaction in the near-threshold region. Calculations of a hypersonic flow over a sphere at 120 km have shown that the number of reactions predicted by QK is significantly higher than QCT due to the strong nonequilibrium, even though the QK rate in a comparable temperature range is somewhat lower than the TCE and QCT.

Of course, a major problem for the TCE approach, or any kinetic model for ultra-high-temperature reacting flows, is the lack of experimental values for the rates in the regime of interest. We caution, as have others in the past, about the extreme unreliability of rate coefficients that are obtained by extrapolating an Arrhenius expression far beyond the temperature at which the parameter values are valid. One strong feature of the QK model is that it is based on the kinetic collision rate coefficient, and so will always properly approach that limit for very high temperatures, in contrast to a mindlessly-extrapolated Arrhenius expression, which in some cases could greatly exceed the kinetic collision limit. An approach worth considering may be to use the QK expressions to provide estimates of $k(T)$ for reactions where no other good values exist, or to provide estimates of the higher temperature regime for reactions where reliable values do not exist at sufficiently high temperatures. These estimated values of $k(T)$ could then be fit to an Arrhenius expression in the range of temperatures relevant to the case of interest, and, if a strongly nonequilibrium flowfield calculation is to be done, the TCE model using the obtained estimated Arrhenius parameters could be used. We are not aware of any disadvantage to this approach.

VI. ACKNOWLEDGMENTS

Support from the Air Force Office of Scientific Research, Dr. Mitat Birkan program manager, is gratefully acknowledged. Dr. Deepak Bose is gratefully acknowledged for providing the complete set of exchange reaction cross sections and permitting their publication here.

[1] G.A. Bird GA, *Molecular Gas Dynamics and the Direct Simulation of Gas Flows,* Clarendon Press, Oxford, 1994.
[2] G.A. Bird, "Simulation of Multi-Dimensional and Chemically Reacting Flows," *Rarefied Gas Dynamics,* Vol. 1, edited by R. Campargue, COMMISSARIAT A LENERGIE ATOMIQUE-Paris 1979, pp. 365-388.
[3] G.A. Bird, "Monte-Carlo simulation in an engineering context," In *Rarefied Gas Dynamics,* ed. S Fisher, Progress in Astronautics and Aeronautics, 1981, vol. 74, pp. 239-255.
[4] M.A. Gallis, R.B. Bond, J.R. Torcyznski, "A Kinetic-theory Approach for Computing Chemical Reaction Rates in Upper Atmosphere Hypersonic Flows," *J. Chem. Phys.*, 2009, Vol. 131, 124311.
[5] M.A. Gallis, R.B. Bond, J.R. Torcyznski, "Assessment of Collision-Energy-Based Models for Atmospheric Species Reactions in Hypersonic Flows," *J. Thermophys. Heat Transf.*, 2010, Vol. 24, No. 2, pp. 241-253.
[6] G.A. Bird, "A Comparison of Collision Energy-Based and Termperature-Based Procedures in DSMC," 26th International Symposium on Rarefied Gas Dynamics, *AIP Conf. Proc.*, 2008, Vol. 1084, 245-250.
[7] M. Capitelli, C. Gorse, S. Longo, D. Giordano, "Collision Integrals of High-Temperature Air Species," *al of Thermophysics and Heat Transfer*, 2000, Vol. 14, No. 2, pp. 259-268.
[8] C. Borgnakke and P.S. Larsen, "Statistical collision model for Monte Carlo simulation of polyatomic gas mixture," *J. Comp. Phys.*, 1975, Vol. 18, pp. 405-420.

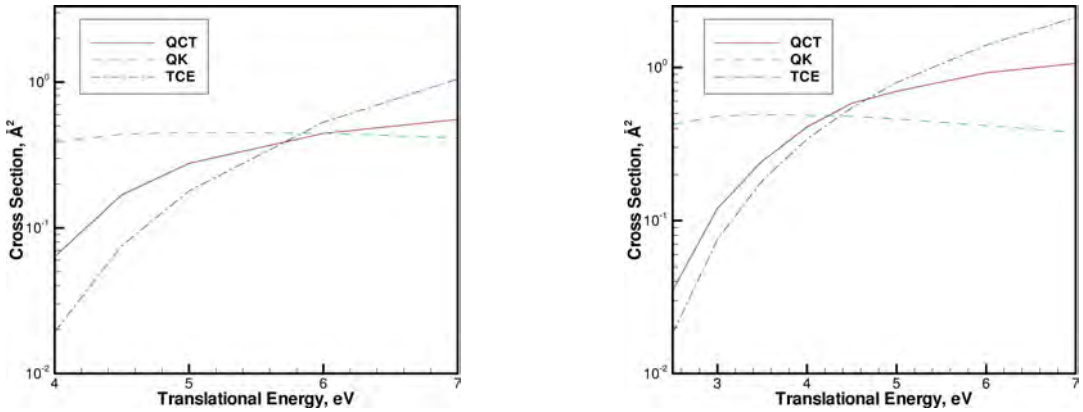

FIG. 10. Exchange reaction cross sections at fixed $J = 0$, $v = 0$ (left) and $J = 0$, $v = 5$ (right).

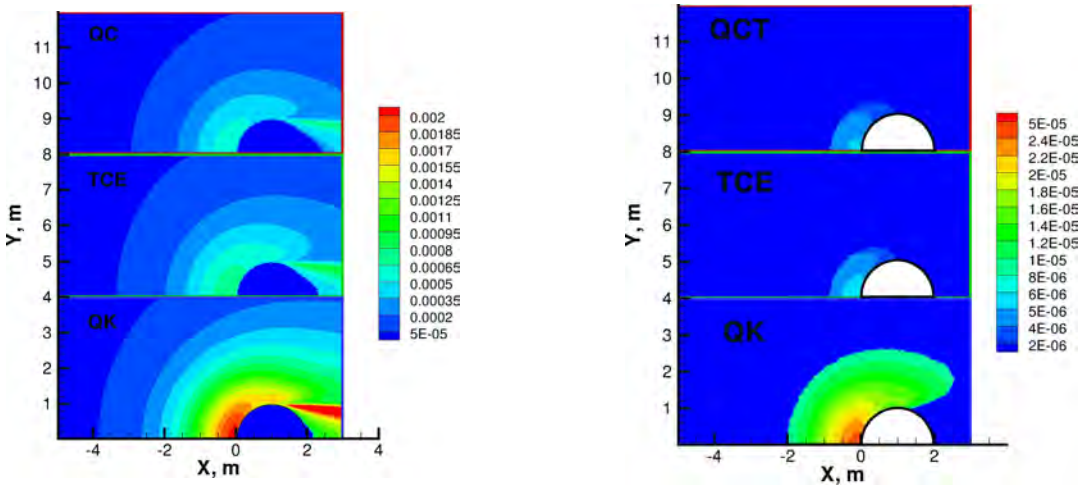

FIG. 11. NO mole fraction in a 8 km/s (left) and 6 km/s (right) flow over a sphere.

[9]D. Bose, G.V. Candler, "Kinetics of the N_2+O← NO+N reaction under thermodynamic nonequilibrium," *J. Thermophys. Heat Transfer*, 1996, Vol. 10, pp. 148-154.

[10]F. Esposito, I. Armenise, M. Capitelli, "N+N_2 state to state vibrational-relaxation and dissociation rates based on quasiclassical calculations," *Chem. Physics*, 2006, Vol. 331, No. 1, pp. 1-8.

[11]S.F. Gimelshein, N. Gimelshein, D.A. Levin, M.S. Ivanov, I.W. Wysong, "On the use of chemical reaction rates with discrete internal energies in the direct simulation Monte Carlo method," *Phys. Fluids*, 2004, Vol. 16, No. 7, pp. 2442-2451.

[12]C. Park, *Nonequilibrium hypersonic aerothermodynamics,* New-York, Wiley&Sons, 1990.

[13]F. Esposito, M. Capitelli, "Quasiclassical molecular dynamic calculations of vibrationally and rotationally state selected dissociation cross-sections: N+N_2(v,j)→3N," *Chemical Physics Letters*, 1999, Vol. 302, pp. 49-54.

[14]F. Esposito, M. Capitelli, C. Gorse, "Quasi-classical dynamics and vibrational kinetics of N+N2(v) system," *Chemical Physics*, 2000, Vol. 257, pp. 193-202.

[15]A. Bourdon , M. Panesi, A. Brandis, T.E. Magin, G. Chaban, W. Huo, R. Jaffe and D.W. Schwenke, "Simulation of flows in shock-tube facilities by means of a detailed chemical mechanism for nitrogen excitation and dissociation," Proceedings of the Summer Program 2008, Center for Turbulence Research, Stanford University, NASA Ames Research Center.

[16]O.P. Shatalov, "Recommended data on rate constants of physical and chemical processes in N-O atoms systems," Moscow State University Russia, Institute of Mechanics, Avogadro Center, Russia, 1987.

[17]D.C. Wadsworth, I.J. Wysong, "Vibrational favoring effect in DSMC dissociation models," *Phys. Fluids*, 1997, Vol. 9, No. 12, pp. 3878-3884.

[18]D.L. Baulch, D.D. Drysdale, D.G. Home, and A.C. Lloyd, *Evaluated Kinetic Data for High Temperature Reactions*, Vol. 1, Butterworth, 1972.

[19]M.S. Ivanov, G.N. Markelov, S.F. Gimelshein, "Statistical simulation of reactive rarefied flows: numerical approach and applications," *AIAA Paper 98-2669.*

[20]D. Bose, "Advanced nitric oxide formation modeling in hypersonic flows," Ph.D. Thesis, Univ. Minnesota, 1997, AAT 9721613.

[21]G.A. Bird, "The Q-K Model for Gas-Phase Chemical Reaction Rates," Submitted to Physics of Fluids, 2011.

TABLE III. $N+N_2 \rightarrow N+N+N$ reaction cross sections in m^2 (averaged over 0.06 eV in translational mode).

E_{tr}, eV \ v	0	3	7	10	20	30	40	50	60	67
					$J = 0$					
0.0643										8.04E-19
0.731								1.17E-22	1.42E-19	7.37E-19
1.40								2.46E-20	2.07E-19	7.10E-19
2.06							9.61E-22	5.91E-20	2.11E-19	6.86E-19
2.73							8.53E-21	7.90E-20	2.09E-19	6.86E-19
3.40						2.38E-22	2.43E-20	7.99E-20	2.21E-19	6.67E-19
4.06						2.04E-21	2.72E-20	1.20E-19	2.19E-19	6.55E-19
4.73						4.11E-21	4.27E-20	1.16E-19	2.20E-19	6.67E-19
5.40						1.26E-20	5.45E-20	1.17E-19	2.25E-19	6.46E-19
6.06					5.49E-22	2.08E-20	6.72E-20	1.20E-19	2.32E-19	6.32E-19
6.73					1.91E-21	2.00E-20	6.20E-20	1.17E-19	2.32E-19	6.50E-19
7.40					3.81E-21	2.48E-20	6.40E-20	1.14E-19	2.18E-19	6.32E-19
8.06					5.15E-21	2.47E-20	7.03E-20	1.24E-19	2.30E-19	6.19E-19
8.73				6.67E-22	9.22E-21	3.66E-20	7.68E-20	1.26E-19	2.30E-19	6.33E-19
9.40				5.94E-22	1.48E-20	4.14E-20	7.19E-20	1.31E-19	2.32E-19	6.19E-19
					$J = 30$					
0.0643									1.11E-21	
0.731								1.68E-21	2.10E-19	
1.40								3.03E-20	2.30E-19	
2.06							3.02E-21	7.05E-20	2.38E-19	
2.73							1.19E-20	8.47E-20	2.32E-19	
3.40						5.40E-22	2.67E-20	1.05E-19	2.57E-19	
4.06						2.41E-21	2.69E-20	1.21E-19	2.35E-19	
4.73						5.21E-21	5.08E-20	1.23E-19	2.47E-19	
5.40					1.13E-22	8.39E-21	5.50E-20	1.23E-19	2.55E-19	
6.06					5.18E-22	2.20E-20	5.88E-20	1.30E-19	2.43E-19	
6.73					1.85E-21	2.56E-20	6.75E-20	1.29E-19	2.44E-19	
7.40					4.20E-21	2.58E-20	6.96E-20	1.32E-19	2.55E-19	
8.06				9.97E-23	5.91E-21	2.92E-20	6.97E-20	1.22E-19	2.53E-19	
8.73			8.95E-23	2.44E-22	1.23E-20	3.58E-20	7.59E-20	1.27E-19	2.44E-19	
9.40			1.55E-22	9.41E-22	1.33E-20	4.57E-20	8.17E-20	1.48E-19	2.67E-19	
					$J = 60$					
0.0643										
0.731								2.66E-20		
1.40							6.11E-22	7.34E-20		
2.06							8.76E-21	9.70E-20		
2.73						9.66E-23	2.43E-20	1.24E-19		
3.40						2.33E-21	3.20E-20	1.30E-19		
4.06						6.47E-21	5.81E-20	1.37E-19		
4.73						1.08E-20	6.20E-20	1.39E-19		
5.40					7.32E-22	2.14E-20	6.86E-20	1.39E-19		
6.06					3.40E-21	2.55E-20	6.82E-20	1.39E-19		
6.73					6.03E-21	2.95E-20	7.94E-20	1.51E-19		
7.40					5.87E-21	3.07E-20	7.85E-20	1.52E-19		
8.06				1.53E-21	1.33E-20	4.75E-20	9.03E-20	1.70E-19		
8.73			1.57E-22	2.22E-21	1.73E-20	4.78E-20	9.06E-20	1.63E-19		
9.40		2.70E-22	1.33E-21	2.81E-21	2.39E-20	5.67E-20	9.66E-20	1.65E-19		
					$J = 90$					
0.0643								2.04E-21		
0.731							2.89E-22	1.23E-19		
1.40							1.20E-20	1.68E-19		
2.06						2.92E-22	3.34E-20	1.86E-19		
2.73						3.25E-21	4.96E-20	2.08E-19		
3.40						6.52E-21	6.19E-20	2.27E-19		
4.06						1.75E-20	7.18E-20	2.14E-19		
4.73					2.13E-21	2.29E-20	8.08E-20	2.06E-19		
5.40					5.53E-21	2.81E-20	9.59E-20	2.13E-19		
6.06					6.80E-21	2.87E-20	9.93E-20	2.04E-19		
6.73				8.95E-23	8.78E-21	4.12E-20	1.12E-19	2.20E-19		
7.40			7.93E-23	8.46E-22	1.42E-20	4.78E-20	1.13E-19	2.09E-19		
8.06		1.29E-22	1.45E-21	2.59E-21	2.23E-20	5.64E-20	1.19E-19	2.10E-19		
8.73		6.55E-22	1.55E-21	3.08E-21	2.18E-20	6.06E-20	1.15E-19	2.20E-19		
9.40	1.55E-22	8.06E-22	2.28E-21	7.03E-21	3.09E-20	7.05E-20	1.15E-19	2.04E-19		
					$J = 120$					
0.0643							8.17E-23			
0.731							3.97E-20			
1.40						1.37E-21	7.70E-20			
2.06						1.05E-20	9.52E-20			
2.73					1.18E-22	2.14E-20	1.16E-19			
3.40					6.28E-22	3.22E-20	1.38E-19			
4.06					6.61E-21	3.56E-20	1.28E-19			
4.73					5.62E-21	4.66E-20	1.31E-19			
5.40				2.44E-22	8.42E-21	6.12E-20	1.43E-19			
6.06			9.19E-23	1.26E-21	1.65E-20	5.87E-20	1.39E-19			
6.73		8.95E-23	1.15E-21	2.79E-21	2.02E-20	6.72E-20	1.45E-19			
7.40	1.16E-22	1.89E-22	1.84E-21	5.86E-21	2.86E-20	6.70E-20	1.59E-19			
8.06	1.50E-22	2.22E-21	3.23E-21	6.48E-21	2.84E-20	7.33E-20	1.63E-19			
8.73	1.33E-21	2.65E-21	3.09E-21	9.90E-21	3.44E-20	8.07E-20	1.61E-19			
9.40	2.17E-21	3.62E-21	6.43E-21	1.32E-20	3.86E-20	8.02E-20	1.78E-19			
					$J = 150$					
0.0643						4.32E-24				
0.731						1.19E-20				
1.40					1.12E-22	3.46E-20				
2.06					2.17E-21	5.11E-20				
2.73					7.42E-21	6.81E-20				
3.40					9.56E-21	7.25E-20				
4.06				8.10E-22	1.81E-20	7.89E-20				
4.73			4.43E-22	1.45E-21	2.71E-20	9.93E-20				
5.40	2.62E-22	1.84E-22	1.43E-21	5.95E-21	2.98E-20	1.05E-19				
6.06	3.63E-22	6.90E-22	3.08E-21	7.05E-21	3.96E-20	1.15E-19				
6.73	8.93E-22	1.76E-21	6.14E-21	6.97E-21	4.06E-20	1.11E-19				
7.40	5.27E-22	2.68E-21	8.27E-21	1.35E-20	5.14E-20	1.31E-19				
8.06	1.79E-21	5.94E-21	1.12E-20	1.92E-20	5.47E-20	1.17E-19				
8.73	4.96E-21	6.02E-21	1.28E-20	1.88E-20	5.82E-20	1.19E-19				
9.40	6.70E-21	9.81E-21	1.52E-20	2.62E-20	6.18E-20	1.19E-19				

TABLE IV. $O+N_2 \rightarrow N+NO$ reaction cross sections in m^2 (calculated by Deepak Bose).

E_{tr}, eV \ v	0	1	3	5	7	10	13
			$J = 0$				
1.2							0.9640E-21
2.0				0.4000E-23	0.2790E-21	0.1595E-20	0.4648E-20
2.5			0.9000E-23	0.3490E-21	0.1216E-20	0.4007E-20	0.8753E-20
3.0			0.3000E-21	0.1200E-20	0.2762E-20	0.6524E-20	0.1163E-19
3.5	0.4700E-22	0.2950E-21	0.1176E-20	0.2437E-20	0.4478E-20	0.8861E-20	0.1390E-19
4.0	0.6480E-21	0.1130E-20	0.2283E-20	0.4082E-20	0.6606E-20	0.1111E-19	0.1555E-19
4.5	0.1682E-20	0.2342E-20	0.3678E-20	0.5833E-20	0.8257E-20	0.1235E-19	0.1716E-19
5.0	0.2768E-20	0.3375E-20	0.4825E-20	0.6979E-20	0.9378E-20	0.1375E-19	0.1899E-19
6.0	0.4438E-20	0.5059E-20	0.6743E-20	0.9218E-20	0.1209E-19	0.1612E-19	0.2022E-19
7.0	0.5442E-20	0.6029E-20	0.8206E-20	0.1061E-19	0.1306E-19	0.1663E-19	0.2035E-19
8.0	0.5950E-20	0.6693E-20	0.8790E-20	0.1101E-19	0.1339E-19	0.1724E-19	0.2016E-19
10.0	0.7069E-20	0.8064E-20	0.1023E-19	0.1223E-19	0.1400E-19	0.1555E-19	0.1692E-19
12.0	0.8007E-20	0.8520E-20	0.9964E-20	0.1099E-19	0.1172E-19	0.1228E-19	0.1250E-19
14.0	0.7742E-20	0.7828E-20	0.8395E-20	0.8959E-20	0.9070E-20		
16.0	0.6903E-20	0.6877E-20	0.6858E-20	0.7070E-20	0.7664E-20		
18.0	0.6165E-20	0.6055E-20	0.6034E-20	0.6301E-20	0.6666E-20		
			$J = 64$				
1.2					0.1300E-22	0.1777E-20	0.6873E-20
2.0			0.2090E-21	0.1235E-20	0.4027E-20	0.1007E-19	0.1684E-19
2.5		0.1380E-21	0.8620E-21	0.2827E-20	0.6275E-20	0.1249E-19	0.1851E-19
3.0		0.7120E-21	0.2115E-20	0.4887E-20	0.8344E-20	0.1416E-19	0.2003E-19
3.5	0.1061E-20	0.1707E-20	0.3761E-20	0.6586E-20	0.1018E-19	0.1556E-19	0.2100E-19
4.0	0.2233E-20	0.3024E-20	0.5481E-20	0.8636E-20	0.1197E-19	0.1682E-19	0.2207E-19
4.5	0.3644E-20	0.4605E-20	0.6938E-20	0.9882E-20	0.1289E-19	0.1787E-19	0.2332E-19
5.0	0.4880E-20	0.5698E-20	0.8122E-20	0.1081E-19	0.1373E-19	0.1892E-19	0.2373E-19
6.0	0.6367E-20	0.7178E-20	0.9717E-20	0.1266E-19	0.1560E-19	0.1964E-19	0.2352E-19
7.0	0.7034E-20	0.7967E-20	0.1039E-19	0.1328E-19	0.1588E-19	0.1964E-19	0.2267E-19
8.0	0.7358E-20	0.8489E-20	0.1095E-19	0.1353E-19	0.1566E-19	0.1877E-19	0.2077E-19
10.0	0.8460E-20	0.9453E-20	0.1129E-19	0.1302E-19	0.1432E-19	0.1537E-19	0.1576E-19
12.0	0.8570E-20	0.9139E-20	0.1020E-19	0.1115E-19	0.1164E-19	0.1205E-19	0.1243E-19
14.0	0.7990E-20	0.8201E-20	0.8671E-20	0.8955E-20	0.9291E-20		
16.0	0.7108E-20	0.7170E-20	0.7412E-20	0.7626E-20	0.7912E-20		
18.0	0.6333E-20	0.6274E-20	0.6360E-20	0.6556E-20	0.6753E-20		
			$J = 90$				
1.2				0.2000E-23	0.5480E-21	0.4069E-20	0.9765E-20
2.0		0.4990E-21	0.1651E-20	0.3973E-20	0.7612E-20	0.1466E-19	0.2218E-19
2.5	0.8240E-21	0.1303E-20	0.3201E-20	0.6728E-20	0.1090E-19	0.1780E-19	0.2513E-19
3.0	0.1640E-20	0.2449E-20	0.5454E-20	0.9324E-20	0.1347E-19	0.2011E-19	0.2678E-19
3.5	0.2849E-20	0.4076E-20	0.7433E-20	0.1133E-19	0.1560E-19	0.2169E-19	0.2709E-19
4.0	0.4467E-20	0.5748E-20	0.9332E-20	0.1316E-19	0.1657E-19	0.2223E-19	0.2807E-19
4.5	0.5961E-20	0.7488E-20	0.1089E-19	0.1395E-19	0.1761E-19	0.2312E-19	0.2872E-19
5.0	0.6899E-20	0.8360E-20	0.1164E-19	0.1498E-19	0.1866E-19	0.2350E-19	0.2797E-19
6.0	0.8232E-20	0.9641E-20	0.1309E-19	0.1625E-19	0.1929E-19	0.2302E-19	0.2646E-19
7.0	0.8995E-20	0.1033E-19	0.1343E-19	0.1609E-19	0.1842E-19	0.2175E-19	0.2423E-19
8.0	0.9573E-20	0.1080E-19	0.1320E-19	0.1553E-19	0.1780E-19	0.1989E-19	0.2124E-19
10.0	0.9792E-20	0.1072E-19	0.1262E-19	0.1398E-19	0.1503E-19	0.1522E-19	0.1576E-19
12.0	0.9337E-20	0.9970E-20	0.1089E-19	0.1149E-19	0.1161E-19	0.1220E-19	0.1274E-19
14.0	0.8274E-20	0.8591E-20	0.8854E-20	0.9219E-20	0.9674E-20		
16.0	0.7290E-20	0.7446E-20	0.7783E-20	0.8020E-20	0.8202E-20		
18.0	0.6554E-20	0.6496E-20	0.6679E-20	0.6825E-20	0.6911E-20		
			$J = 110$				
1.2				0.3940E-21	0.2571E-20	0.7317E-20	0.1401E-19
2.0	0.1402E-20	0.1793E-20	0.3950E-20	0.7478E-20	0.1220E-19	0.1985E-19	0.2802E-19
2.5	0.2682E-20	0.3663E-20	0.6976E-20	0.1148E-19	0.1642E-19	0.2365E-19	0.3152E-19
3.0	0.3998E-20	0.5764E-20	0.1001E-19	0.1431E-19	0.1887E-19	0.2622E-19	0.3323E-19
3.5	0.5896E-20	0.7919E-20	0.1208E-19	0.1644E-19	0.2083E-19	0.2688E-19	0.3363E-19
4.0	0.7746E-20	0.9786E-20	0.1388E-19	0.1787E-19	0.2175E-19	0.2780E-19	0.3404E-19
4.5	0.9043E-20	0.1120E-19	0.1474E-19	0.1860E-19	0.2239E-19	0.2850E-19	0.3278E-19
5.0	0.1013E-19	0.1180E-19	0.1559E-19	0.1941E-19	0.2344E-19	0.2781E-19	0.3118E-19
6.0	0.1115E-19	0.1308E-19	0.1672E-19	0.1975E-19	0.2215E-19	0.2577E-19	0.2892E-19
7.0	0.1174E-19	0.1340E-19	0.1609E-19	0.1869E-19	0.2114E-19	0.2407E-19	0.2577E-19
8.0	0.1179E-19	0.1312E-19	0.1558E-19	0.1776E-19	0.1943E-19	0.2107E-19	0.2150E-19
10.0	0.1109E-19	0.1218E-19	0.1385E-19	0.1490E-19	0.1555E-19	0.1576E-19	0.1646E-19
12.0	0.9999E-20	0.1066E-19	0.1125E-19	0.1199E-19	0.1201E-19	0.1248E-19	0.1276E-19
14.0	0.8774E-20	0.8993E-20	0.9384E-20	0.9851E-20	0.1011E-19		
16.0	0.7654E-20	0.7725E-20	0.8000E-20	0.8137E-20	0.8301E-20		
18.0	0.6632E-20	0.6693E-20	0.6788E-20	0.6819E-20	0.6992E-20		
			$J = 126$				
1.2			0.3540E-21	0.2489E-20	0.5267E-20	0.1152E-19	0.1897E-19
2.0	0.2695E-20	0.3957E-20	0.7721E-20	0.1240E-19	0.1780E-19	0.2612E-19	0.3440E-19
2.5	0.5585E-20	0.7357E-20	0.1187E-19	0.1701E-19	0.2203E-19	0.2989E-19	0.3812E-19
3.0	0.8085E-20	0.1027E-19	0.1501E-19	0.1940E-19	0.2476E-19	0.3161E-19	0.3907E-19
3.5	0.1024E-19	0.1238E-19	0.1711E-19	0.2155E-19	0.2586E-19	0.3286E-19	0.3959E-19
4.0	0.1201E-19	0.1424E-19	0.1821E-19	0.2229E-19	0.2672E-19	0.3311E-19	0.3801E-19
4.5	0.1288E-19	0.1512E-19	0.1918E-19	0.2344E-19	0.2742E-19	0.3206E-19	0.3595E-19
5.0	0.1368E-19	0.1580E-19	0.2009E-19	0.2414E-19	0.2720E-19	0.3058E-19	0.3443E-19
6.0	0.1465E-19	0.1652E-19	0.1990E-19	0.2254E-19	0.2509E-19	0.2876E-19	0.3099E-19
7.0	0.1476E-19	0.1624E-19	0.1874E-19	0.2136E-19	0.2346E-19	0.2552E-19	0.2656E-19
8.0	0.1414E-19	0.1547E-19	0.1782E-19	0.1974E-19	0.2103E-19	0.2206E-19	0.2222E-19
10.0	0.1257E-19	0.1332E-19	0.1466E-19	0.1539E-19	0.1599E-19	0.1637E-19	0.1703E-19
12.0	0.1093E-19	0.1147E-19	0.1211E-19	0.1239E-19	0.1281E-19	0.1285E-19	0.1291E-19
14.0	0.9206E-20	0.9603E-20	0.1007E-19	0.1001E-19	0.1032E-19		
16.0	0.7913E-20	0.8105E-20	0.8309E-20	0.8472E-20	0.8512E-20		
18.0	0.6856E-20	0.6770E-20	0.6734E-20	0.6931E-20	0.7148E-20		